Frequency-selective surfaces with multiple apertures within a periodic cell

Jeffrey A. Reed

School of Natural Sciences and Mathematics, The University of Texas at Dallas, Richardson, Texas 75083

Dale M. Byrne

Erik Jonsson School of Engineering and Computer Science, The University of Texas at Dallas, Richardson, Texas 75083

Received October 1, 1997; accepted October 6, 1997

We discuss a method for analyzing frequency-selective surfaces (FSS's) consisting of an array of multiple apertures or patches per unit periodic cell. Based on the modal method, our method is unique in that the multiple apertures or patches within a unit cell need not be identical in size or shape. Applying our technique to thin perfectly conducting sheets perforated with patterns of varying-length narrow rectangular apertures, we demonstrate a pattern of slot apertures that produces a double-resonance spectral transmission profile.
 [S0740-3232(98)00203-8]
OCIS codes: 040.1240, 050.1940, 050.2770, 290.0290.

1. INTRODUCTION

A conducting sheet periodically perforated with apertures, or an array of periodic metallic patches, constitutes a frequency-selective surface (FSS) to electromagnetic waves. There are two generic geometries that are typically discussed in the literature. The first geometry, commonly referred to as an inductive FSS, performs similarly to a high-pass filter. The second case, or capacitive FSS, is similar to a low-pass filter. If the periodic elements within an FSS possesses resonance characteristics, the inductive FSS will exhibit total transmission at wavelengths near the resonant wavelength, while the capacitive FSS will exhibit total reflection. This feature allows an FSS with the proper elements to perform as a narrow-bandpass filter. It therefore becomes desirable to understand the relationship among the element shape, the periodic array geometry, and the resonance behavior in order to construct narrow-bandpass filters out of frequency-selective surfaces.

If one considers a wavelength region where the wavelength is much larger than the FSS thickness, an infinitely thin approximation may be employed. Many FSS's are constructed with printed-circuit-type elements where the thickness of the elements is much less than the resonant wavelength so that the infinitely thin approximation will be valid. Obviously, metallic patches cannot be deposited into free space, so they usually are deposited on a dielectric layer. Thin conducting sheets perforated with apertures also need to be deposited on a substrate for support. The effect of this dielectric layer must also be taken into account when one is analyzing the response of the filter. Since this adds another level of complexity to the problem, the theoretical case of the FSS in free space (no dielectric layer present) is often used as a starting point to model the frequency response of the filter. Once this free-space model is understood, it becomes a straightforward process to account for the effects of the dielectric layers necessary in an actual filter.

Much work has been done in the area of analyzing the frequency response of thin periodic interfaces. The method for analyzing these frequency-selective surfaces can be broken down into three main categories: circuit theory techniques, modal expansion techniques, and iterative techniques. The circuit-theory approach utilizes the quasi-static approximation to derive the equivalent circuit model for the FSS. An example of this approach is provided by Ulrich[1] for thin metallic mesh grids and their complimentary structures. In the modal expansion technique, Floquet modes in space (diffracted orders) are matched with the aperture modes (or current modes) to form an integral equation. This integral equation is solved by a technique such as the method of moments[2] or the conjugate-gradient technique.[3] With iterative methods[4] one can avoid large matrix storage requirements by utilizing iteration to avoid explicitly computing the matrices. In the spectral iterative technique, the current on the surface of the conducting region is the quantity being iterated. The merits of the various techniques are discussed by Wu.[5] A survey of analytical methods applied to periodic gratings is described by Petit.[6]

In previous papers analyzing frequency-selective surfaces, all apertures (or patches) were identical and arranged in a periodic fashion. We consider an extension to this case, where groups of N apertures are arranged in a periodic array. Specifically, we consider rectangular apertures with N equal to 2. In the results presented here, we show a periodic array geometry that possesses a double-resonance character, similar in general form to that presented by Munk and Luebbers.[7] Their results

differ from those presented here in that they considered the reflection characteristics of two interlaced arrays of different length dipoles, whereas we consider the transmission characteristics of various slot array geometries.

2. MATHEMATICAL FORMULATION

Since we were interested in modeling planar mesh geometries, also referred to as thin meshes, it was decided to adapt the modal method of Chen[8] to the case of multiple apertures per periodic cell. Chen's modal method is well suited to rectangular apertures, with the basis functions that are used to expand the field in each aperture being rectangular waveguide modal functions. All resulting coefficient integrals can then be expressed in closed form, speeding up numerical computation considerably.

Chen's method makes use of the fact that the periodic aperture geometry imposes a periodicity on the scattered wave fields near the filter surface. To model this periodicity the incident, reflected, and transmitted transverse electric fields are expanded in terms of Floquet modes, $\bar{\Phi}$, with unknown reflection and transmission coefficients, R and B included in the formulation. By using modal orthogonality, Chen solved for the unknown coefficients that represent the amplitudes of the Floquet modes in terms of an integral relation of the unknown field and each Floquet mode. Substituting the integral relation for the coefficients R and B, Chen obtained an integral equation for the unknown field distribution. Starting with this integral equation, we began our modifications to extend Chen's method to periodic groups of apertures based on a similar approach by Amitay *et al.*[9]

Our analysis applies to the idealized case of a perfectly conducting, infinitely thin metal filter perforated with identical groups of N apertures as shown in Fig. 1. Each group constitutes a periodic cell within the filter. Although each group is identical and arranged in a periodic fashion, each member aperture of the group need not be identical. The field in each aperture is expanded in a set of vector orthonormal functions $\bar{\Psi}$, satisfying the aperture boundary conditions. The set of $\bar{\Psi}$'s are the standard waveguide modes suitable for a waveguide that has the cross-sectional shape of the aperture. With the notation of Chen,[8] the waveguide expansion of the transverse electric field at the surface of the filter ($z = 0$), contributed by the apertures is

$$\bar{E}_t = \sum_{i=1}^{N} \bar{E}_t^{(i)} = \sum_{i=1}^{N} \sum_{l=1}^{2} \sum_{m} \sum_{n} F_{mnl}^{(i)} \bar{\Psi}_{mnl}^{(i)}, \qquad (1)$$

where the superscript i denotes the ith type of aperture within a group, and the subscripts m, n, and l denote the mn-expansion mode for TE polarization ($l = 1$) or TM polarization ($l = 2$).

For the case of a single aperture per periodic cell ($N = 1$), the integral equation (which must be satisfied over the aperture only), as derived by Chen[7] [Eq. (13)], is

$$2\sum_{r=1}^{2} A_{00r}\xi_{00r}\bar{\Phi}_{00r} = \sum_{p}\sum_{q}\sum_{r=1}^{2} (\xi_{pqr} + Y_{pqr}) \times \bar{\Phi}_{pqr} \int\int_{\text{aperture}} \bar{E}_t \cdot \bar{\Phi}_{pqr}^{*} \mathrm{d}a, \qquad (2)$$

where A is the incident-plane-wave expansion coefficient, ξ is the modal admittance, Y is the modal admittance of a dielectric substrate if present ($Y = \xi$ for no substrate), $\bar{\Phi}_{pqr}$ is the vector pq-Floquet mode for the TE polarization ($r = 1$) or TM polarization ($r = 2$) in the free-space region ($z < 0$), and * denotes the complex conjugate. It should be noted that the integral in Eq. (2) is over the entire unit cell. However, since $\bar{E}_t = 0$ on the metal surface for a perfect conductor, this integral reduces to the requirement that it be satisfied only over the aperture region. Thus Eq. (2) is also valid for any periodic group of

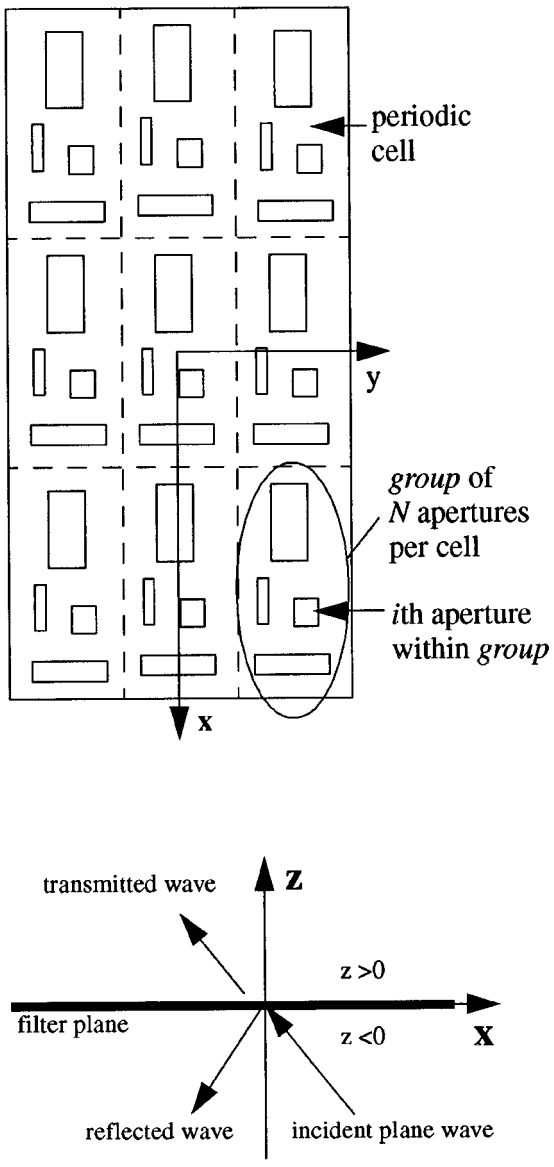

Fig. 1. Typical geometric configuration for a FSS with multiple apertures within a periodic cell.

N apertures since at the filter plane there would be only a field within the apertures and no field on the perfect conductor between the apertures within the group.

The derivation of the matrix expression for the unknown coefficients begins by inserting Eq. (1) into Eq. (2). One then multiplies both sides of Eq. (2) by $\bar{\Psi}^*_{m'n'l'}$ and integrates over the ith aperture to obtain the integral equation for the ith aperture within a periodic group of N apertures

$$2\sum_{r=1}^{2} A_{00r}\xi_{00r}C_{00r}^{(i)m'n'l'*} = \sum_{p}\sum_{q}\sum_{r=1}^{2} G_{pqr}C_{pqr}^{(i)m'n'l'*} \times \left(\sum_{j=1}^{N}\sum_{m}\sum_{n}\sum_{l=1}^{2} F_{mnl}^{(j)}C_{pqr}^{(j)m'n'l'}\right), \quad (3)$$

where

$$G_{pqr} = \xi_{pqr} + Y_{pqr}, \quad (4)$$

$$C_{pqr}^{(j)m'n'l'} = \int\int_{j\text{th-aperture}} \bar{\Psi}^{j}_{m'n'l'} \cdot \bar{\Phi}^*_{pqr}\,da. \quad (5)$$

Equation (3) generates N systems of linear algebraic equations,

$$2(I_{m_i'n_i'l_i'}^{(i)}) = \sum_{j=1}^{N} (Y_{m_i'n_i'l_i'}^{(i,j)m_jn_jl_j})(F_{m_jn_jl_j}^{(j)}), \quad (6)$$

which may be combined into one large system of equations, of the general form

$$2[I] = [Y][F]. \quad (7)$$

The matrix elements in the above expression are given by

$$Y_{m_i'n_i'l_i'}^{(i,j)m_jn_jl_j} = \sum_{p}\sum_{q}\sum_{r=1}^{2} G_{pqr}(C_{pqr}^{(i)m_i'n_i'l_i'})^*C_{pqr}^{(j)m_jn_jl_j} \quad (8)$$

$$I_{m_i'n_i'l_i'}^{(i)} = \sum_{r=1}^{2} A_{00r}\xi_{00r}(C_{00r}^{(i)m_i'n_i'l_i'})^*. \quad (9)$$

The resulting matrix Eq. (7) can then be solved for the unknown coefficients F, which from Eq. (1) yield the transverse electric field at the surface of the mesh.

Finally, the reflection coefficients R_{pqr} and the transmission coefficients B_{pqr} can be found from the relationship

$$\delta_{0p}\delta_{0q}A_{pqr} + R_{pqr} = B_{pqr} = \sum_{j=1}^{N}\left(\sum_{m_j}\sum_{n_j}\sum_{l_j} F_{m_jn_jl_j}^{(j)}C_{pqr}^{(j)m_jn_jl_j}\right), \quad (10)$$

where δ is the Kronecker delta.

An advantage of this method is that it seems to avoid the problem of series truncation for sets of multiple periodic equations as described by Mittra.[10] In theory, the modal expansions for the ith aperture $\bar{\Psi}^{(i)}$ are infinite but for computational reasons are truncated at a point that provides relative convergence of the resulting reflection and transmission coefficients. For a single aperture per periodic cell there is only one series to truncate, but for multiple apertures per periodic cell there is an expansion for each of the apertures within the periodic cell that must be truncated. As a result of this multiple partitioning, the coefficients R_{pqr} and B_{pqr} could converge to multiple values depending on the choice of truncation points. To confirm that this problem with multiple partitioning was not occurring, we varied the modal expansions between 6 and 14 terms for each of the apertures within a periodic cell and looked at the resulting R_{pqr} and B_{pqr}. For the cases of apertures being in the form of a narrow slot, the coefficients R_{pqr} and B_{pqr} converged relatively smoothly to one value, with a choice of 10 terms for all modal expansions $\bar{\Psi}^{(i)}$ appearing as optimal for relative convergence/computational time considerations.

This method may also be extended to circular apertures by using circular waveguide modes as the expansion functions in Eq. (1) as in the $N = 1$ case described by Chen.[11] Capacitive filters (metal patches as opposed to apertures) can be analyzed by applying the above procedure as described by Chen,[12] Montgomery,[13] and Dawes *et al.*[14] A program was written in Fortran for a Sun workstation by using the above modifications of Chen's method to analyze a filter consisting of up to $N = 4$ different rectangular apertures per periodic cell. Although this paper deals exclusively with rectangular aperture geometries in free space, the program can also analyze filters with circular apertures and filters on dielectric substrates and/or superstrates, as well as the equivalent capacitive filters in a variety of configurations.

3. RESULTS

Our basic goal was to model the spectral and polarization characteristics of frequency-selective surfaces consisting of groups of nonsimilar apertures arranged in a periodic fashion. Narrow rectangular apertures were chosen as a starting point, since these have been shown to exhibit relatively narrow bandpass characteristics that are polarization dependent. The baseline filter geometry used for all comparisons is shown in Fig. 2(a). This filter consisted of an infinitely thin, perfectly conducting surface, perforated by 5.0 μm $\times$ 0.5 μm rectangular apertures. The apertures were arranged periodically with a spacing of 6.0 μm in both the x and y directions. For a rectangular array, the element spacing is often referred to as the diffraction edge since all diffracted orders are evanescent except for the zero or specular order for wavelengths larger than this value. A normally incident plane wave was considered to be impinging on the surface, and the resulting transmission profile was calculated. In this paper TE polarization refers to the case in which the electric field is perpendicular to the long dimension of the aperture. As shown in Fig. 2(b), the baseline example produces a bandpass transmission profile. This profile is typical for the case of TE polarization and illustrates the concept that for wavelengths larger than the element spacing, the spectral characteristic is determined to a large extent by the aperture shape. The slot aperture has been shown to produce a transmission bandpass, with

the wavelength of peak transmission approximately equal to 2.1 times the slot length[15] (when the filter is in air).

A. Varying Aperture Length in Alternating Columns

Our first modification to the baseline geometry shown in Fig. 2(a) consisted of rectangular apertures in which the longer dimension differed for slots in alternate columns. The rationale for this geometry is that since an array of identical slots produces a transmission profile that is dependent on the slot length, combining two arrays of differing slot lengths might produce a transmission profile with a dual bandpass feature. Figure 3(a) shows this filter layout. In all of our numerical computations, the aperture dimensions $a_1 = 5.0\ \mu$m and $b_1 = b_2 = 0.5\ \mu$m remained constant. We considered aperture lengths for the shorter apertures in the range between $a_2 = 4.0\ \mu$m and $a_2 = 5.0\ \mu$m in 0.25-μm increments. Note that when $a_2 = 5.0\ \mu$m, the geometry is identical to the original baseline geometry. Although individual apertures were still separated by 6.0 μm, the group periodicity in the y direction, d_y, became 12.0 μm, and each periodic cell now consisted of two apertures instead of one as in the baseline case. Again we considered a normally incident plane wave with TE polarization.

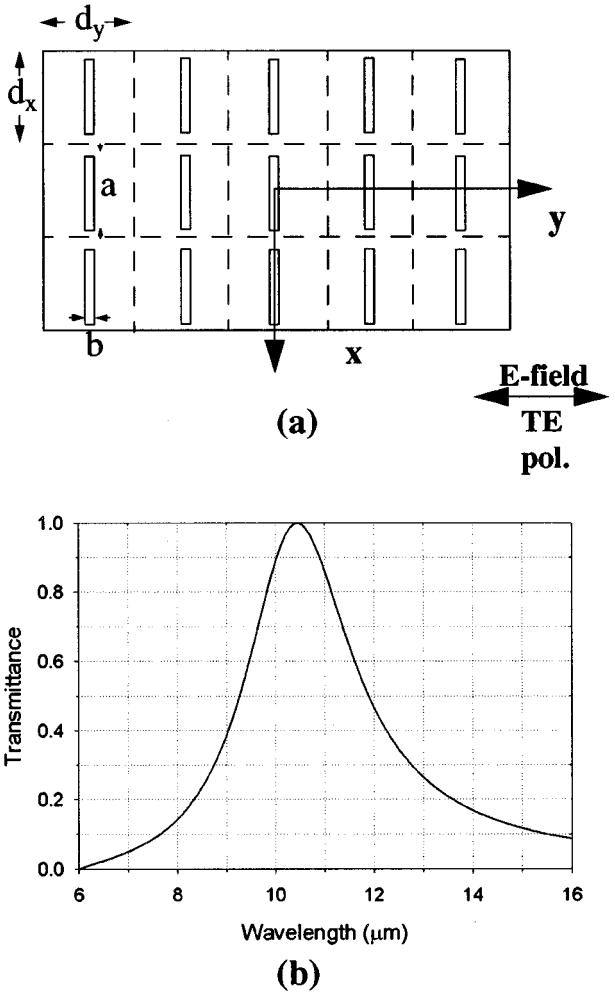

Fig. 2. (a) FSS geometry used as the baseline configuration. (b) Zeroth-order transmission spectral profile for the baseline configuration of (a). In this example $d_x = d_y = 6.0\ \mu$m, $a = 5.0\ \mu$m, and $b = 0.5\ \mu$m.

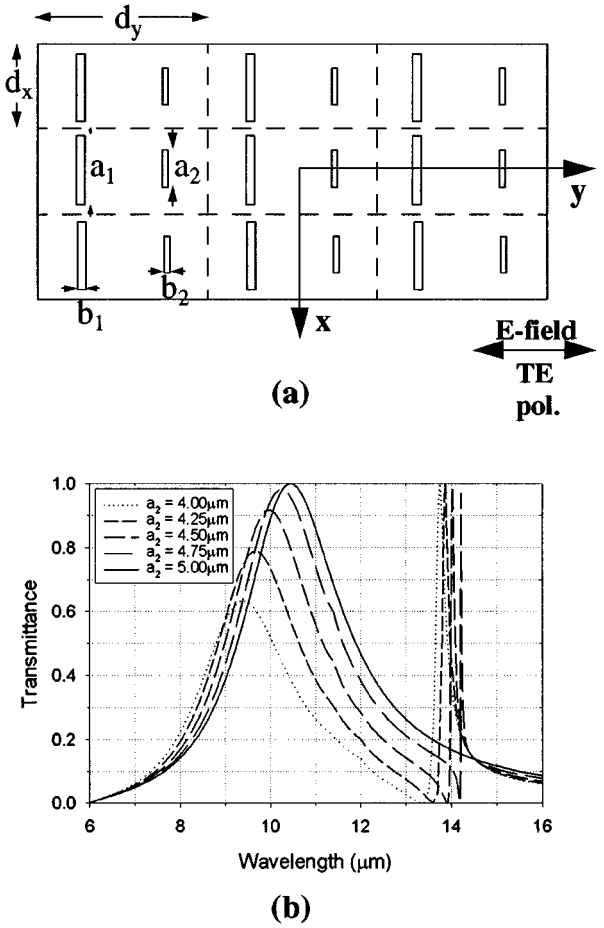

Fig. 3. (a) Geometry used for a FSS consisting of a rectangular array of two different apertures per periodic cell (columns of long slots alternate with columns of short slots). (b) Zeroth-order transmission spectral profiles for (a) with the short slot apertures ranging in length from $a_2 = 4.0\ \mu$m to $a_2 = 5.0\ \mu$m ($b_2 = 0.5\ \mu$m). The long slot apertures were constant at $a_1 = 5.0\ \mu$m and $b_1 = 0.5\ \mu$m; the periodicity was $d_x = 6.0\ \mu$m and $d_y = 12.0\ \mu$m.

The resulting transmission profiles are presented in Fig. 3(b). The resulting profiles differ dramatically from our baseline profile [the solid curve in Fig. 3(b)]. Instead of a single resonance peak, the new profiles exhibit a dual resonance, consisting of a broad peak with a bandwidth (full width at half-maximum) on the order of 2 μm, and a narrow peak with a bandwidth on the order of 0.2 μm. The broad resonance bandwidth increases from 2.2 to 3.0 μm as a_2 increases from 4.0 to 5.0 μm. Also, as a_2 increases from 4.0 to 5.0 μm, the wavelength of maximum transmission of the broad resonance increases from approximately 9.3 μm to 10.4 μm, while its maximum transmittance value increases from 0.63 to 1.0. Since the periodicity in the y direction is 12.0 μm, orders other than the specular order are propagating in the far field for wavelengths less than 12.0 μm. We note that since all of the broad resonance peaks occur at wavelengths *less* than 12.0 μm, the resonance peaks would not be expected to approach a maximum value of 1.0, because some energy propagates in diffracted orders other than the specular

order. The lone exception is for $a_2 = 5.0\ \mu$m, which reverts to our baseline geometry, with a periodicity of 6.0 μm in the y direction. Only the specular order is propagating in the far field for the wavelengths greater than 6.0 μm for this configuration. Consequently, the resonance peak is expected to reach a maximum value of 1.0 for this case.

It should be noted that all of the narrow resonance peaks occur at wavelengths greater than 12.0 μm, where only the specular order is propagating in the far field. In this spectral region, all of the narrow peaks should approach a maximum value of 1.0, which indeed they do. An interesting feature is the decreasing bandwidth that results as a_2 increases from 4.0 to 5.0 μm. At $a_2 = 4.0\ \mu$m the bandwidth is 0.25 μm, whereas at $a_2 = 4.75\ \mu$m, it has decreased to less than 0.03 μm. Of course, for $a_2 = 5.0\ \mu$m, our baseline geometry, no narrow peak is present. The implication is that as a_2 approaches a_1 for this type of filter geometry, the resulting resonance bandpass increasingly narrows. In addition, the wavelength of maximum transmission shifts monotonically toward longer wavelengths as a_2 increases. The specific manner in which the bandwidth and the spectral location of both resonances vary will be discussed in a subsequent paper. In any case, this feature may prove valuable in the design of a very-narrow-bandpass filter.

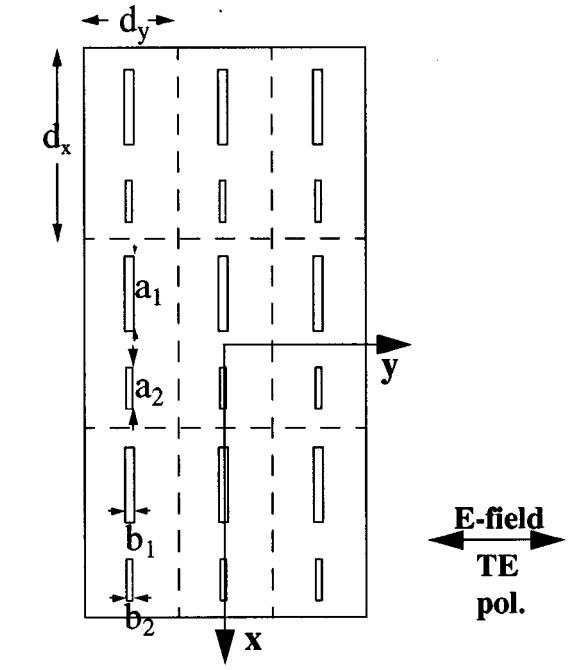

(a)

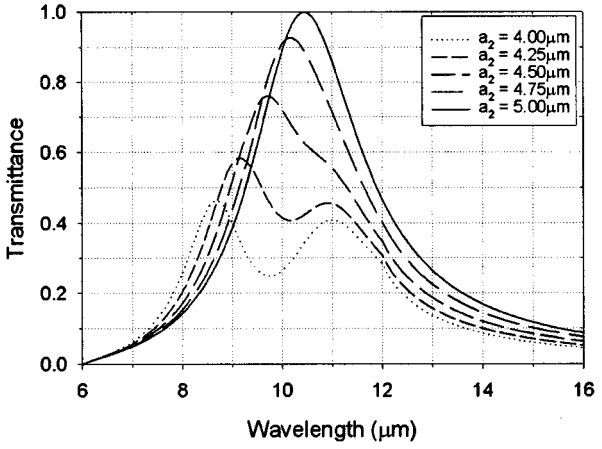

(b)

Fig. 4. (a) Geometry used for a FSS consisting of a rectangular array of two different apertures per periodic cell (rows of long slots alternate with rows of short slots). (b) Zeroth-order transmission spectral profiles for (a) with the short slot apertures ranging in length from $a_2 = 4.0\ \mu$m to $a_2 = 5.0\ \mu$m ($b_2 = 0.5\ \mu$m). The long slot apertures were constant at $a_1 = 5.0\ \mu$m and $b_1 = 0.5\ \mu$m; the periodicity was $d_x = 12.0\ \mu$m and $d_y = 6.0\ \mu$m.

B. Varying Aperture Length in Alternating Rows

A second modification of the baseline geometry consisted of varying the aperture length in alternating rows as shown in Fig. 4(a). Again $a_1 = 5.0\ \mu$m and $b_1 = b_2 = 0.5\ \mu$m was constant throughout all computations, while a_2 was varied as in the previous example from 4.0 to 5.0 μm. The periodicity in the y direction, d_y, is 6.0 μm, but the cell or group periodicity in the x direction, d_x, has increased to 12.0 μm. Again, a periodic cell consists of two apertures. Figure 4(b) shows the transmission profiles resulting from a normally incident plane wave with TE polarization.

The spectral profiles for this filter geometry are quite different from the baseline geometry and from those in the previously discussed case. No pronounced dual resonance peaks are observed. In fact, no resonance peaks occur at all for wavelengths greater than 12.0 μm (the wavelength region where only the specular order is propagating in the far field). Several of the profiles have minor dips in the wavelength range from 6.0 to 12.0 μm, but overall, there are no dramatic resonance type characteristics that might be exploited in a bandpass filter design. On the other hand, one could consider the bandwidth of the passband to be widened. There must be further study to determine whether there are ways to smooth the "within-band" transmissivity and/or sharpen the fall-off.

C. Varying Aperture Length in Alternating Rows and Columns

We next investigated the effect of varying the aperture length in alternating rows and alternating columns to create the mesh geometry shown in Fig. 5(a). This particular geometry requires the periodic group to have two member apertures arranged in a triangular array. In this arrangement the periodicity is 12.0 μm along the x axis and 6.0 μm along the y axis. However, the periodicity of $6\sqrt{2}\ \mu$m along the skewed axis y' defines the diffraction edge λ_d. The normally incident plane wave is again assumed to be TE polarized. As with the previous two examples, the long slot is held constant with dimensions $a_1 = 5.0\ \mu$m, $b_1 = 0.5\ \mu$m. The short slot has $b_2 = 0.5\ \mu$m, also held constant, while a_2 is incremented from 0.5 to 5.0 μm. Note that when $a_2 = 5.0\ \mu$m, all

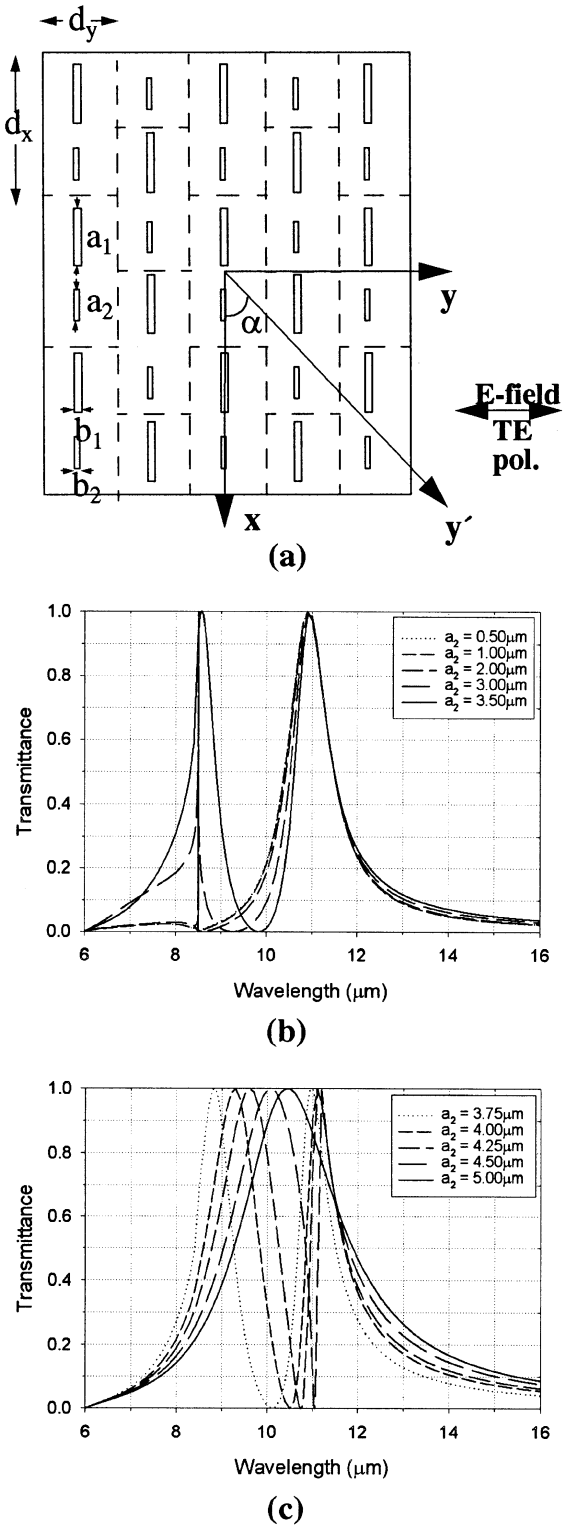

Fig. 5. (a) Geometry used for a FSS consisting of a triangular array of two different apertures per periodic cell (long slots alternate with short slots). (b) Zeroth-order transmission spectral profiles for (a) with the short slot apertures ranging in length from $a_2 = 0.5\ \mu$m to $a_2 = 3.5\ \mu$m ($b_2 = 0.5\ \mu$m). The long slot apertures were constant at $a_1 = 5.0\ \mu$m and $b_1 = 0.5\ \mu$m; the periodicity was $d_x = 12.0\ \mu$m, $d_y = 6.0\ \mu$m, and $\alpha = 45°$. (c) Zeroth-order transmission spectral profiles for (a) with the short slot apertures ranging in length from $a_2 = 3.75\ \mu$m to $a_2 = 5.0\ \mu$m. All other dimensions are the same as in (b). The dual-resonance nature of the FSS is clearly evident in this figure.

slots are identical, and the array is the baseline configuration depicted in Fig. 2(a). For clarity, the spectral profiles are separated into two figures. The spectral profiles shown in Fig. 5(b) result from the mesh geometries in which the short slot dimensions lie between $a_2 = 0.5\ \mu$m and $a_2 = 3.5\ \mu$m, while the spectral profiles shown in Fig. 5(c) result from geometries in which the short slot dimensions are between $a_2 = 3.75\ \mu$m and $a_2 = 5.0\ \mu$m.

The profiles in Fig. 5(b) show a single resonance peak located near 10.9 μm for all of the cases of a_2 between 0.5 and 3.50 μm. In addition, each curve exhibits a transmission peak at a wavelength just short of the diffraction edge wavelength of $\lambda_d = 6\sqrt{2}\ \mu$m. This resonance peak is the familiar Wood's anomaly reported frequently in the literature.[16–23] Although they are not clearly depicted in Fig. 5(b), rapid variations (as a function of wavelength) due to Wood's anomalies do occur for the case of $a_2 = 3.50\ \mu$m when the curves are inspected in finer detail for wavelengths near $6\sqrt{2}\ \mu$m.

All of the spectral profiles in Fig. 5(c) exhibit a dual resonance nature. As a_2 is varied from 3.75 to 4.50 μm, the shorter-wavelength resonance peak shifts from 8.8 to 10.1 μm, while the second resonance peak shifts very slightly between 11.0 and 11.1 μm. It should also be noted that no classical Wood's anomalies are observed for these cases of a_2 between 3.75 and 5.00 μm.

D. Further Comments on Wood's Anomalies

To investigate further the presence or absence of Wood's anomalies, we next investigate three generically similar mesh geometries of 0.5 μm × 5.0 μm slots. Figure 6(a) depicts a square array of slots spaced $6\sqrt{2}\ \mu$m along both the x and the y axes. In Fig. 6(b) the slots are arranged in a triangular array with the spacing along the skewed axis at $6\sqrt{2}\ \mu$m. Finally, in Fig. 6(c), slots rotated by 90° are added interstitially between the slots in Fig. 6(b). In all three arrays the diffraction edge is located at a wavelength of $6\sqrt{2}\ \mu$m (the distance between nearest neighbors). The transmission spectral profiles for all three arrays are presented in Fig. 6(d).

Since all three arrays have narrow slots, they would be expected to produce a resonance effect similar to that of our baseline geometry. By application of Babinet's principle, a complementary strip dipole array will produce a reflection profile identical to the transmission profile of a narrow slot array. Chase and Joseph[15] have given the resonant wavelength λ_r of a single flat strip dipole (no substrate) of length L and width b as

$$\lambda_r = 2.1\left(1 + \frac{b}{2L}\right)L. \tag{11}$$

For a flat strip dipole of dimensions 0.5 μm × 5.0 μm, λ_r should be 11.025 μm. This resonant wavelength value should correspond to the resonance wavelength in a complimentary array of narrow slots by application of Babinet's principle. Figure 6(d) shows λ_r to be approximately 11 μm for the three slot arrays of Figs. 6(a)–6(c). As Chase and Joseph note, the mutual impedance between adjacent elements of an array of dipoles will alter the resonant wavelength from that of a single dipole given in

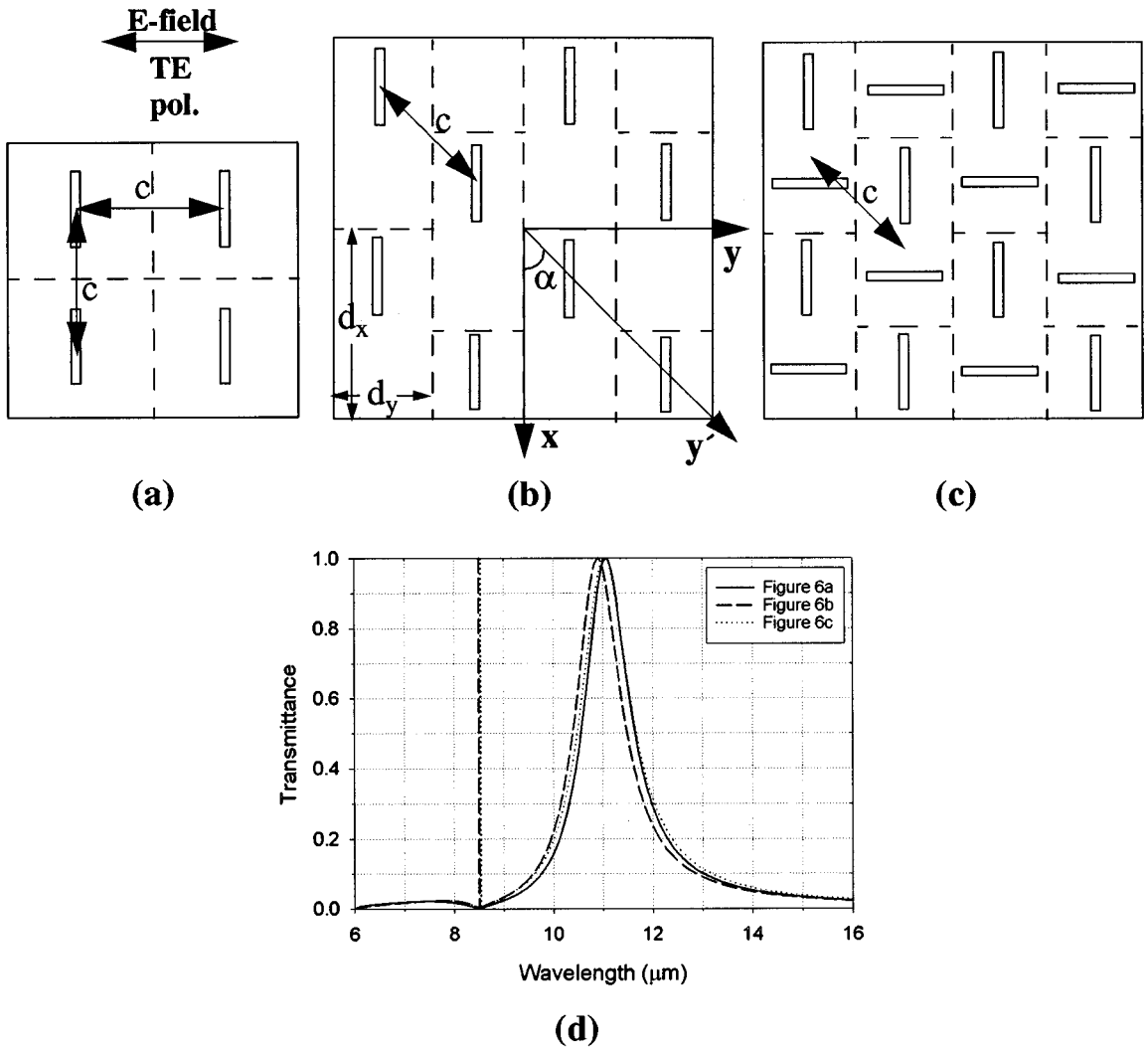

Fig. 6. (a) FSS with rectangular array of slot apertures. Slot dimensions were 5.0 μm $\times$ 0.5 μm with period $c = 6\sqrt{2}$ μm. (b) FSS with triangular array of slot apertures. Slot dimensions are the same as Fig. 6(a) with period $d_x = 12.0$ μm and $d_y = 6.0$ μm ($\alpha = 45°$). The nearest-neighbor distance is $c = 6\sqrt{2}$ μm. (c) FSS with triangular array of two different apertures per periodic cell (alternating slots rotated 90°). Slot dimensions and periodicity are the same as in (b). (d) Zeroth-order transmission spectral profiles for (a)–(c).

Eq. (11). However, for the arrays in Figs. 6(a)–6(c), the effect of mutual impedance between the slots seems to be negligible. Clearly, the resonance effect in these three transmission spectral profiles is due to the dipole-like nature of the slots.

Additional observations indicate that the rectangular array shown in Fig. 6(a) does not exhibit a Wood's anomaly at the diffraction edge wavelength of $6\sqrt{2}$ μm, whereas both of the triangular arrays [Figs. 6(b) and 6(c)] do exhibit an anomaly. Also, the addition of the rotated slots in Fig. 6(c) has little effect on the transmission spectral profile. Since the E field is polarized along the direction of these rotated dipole-like slots, the slots insignificantly modify the transmission spectral profile, because the current path induced by the incident field experiences only minor perturbations as a result of the presence of the horizontal slots. Similarly, variation of the length of these rotated slots should also have little effect on the transmission spectral profile since the slots are narrow.

If the length of these rotated slots were decreased to 0.5 μm, they would become very small squares, and the resulting array would be identical to that in Fig. 5(a) for the case of $a_2 = 0.5$ μm. Consequently, the array in Fig. 6(c) should produce a transmission spectral profile similar to that in Fig. 5(b) for $a_2 = 0.5$ μm. Comparison of the transmission spectral profile in Fig. 6(d) shows it to be nearly identical to the one in Fig. 5(b) for $a_2 = 0.5$ μm.

As a_2 is increased from 0.5 to 3.50 μm in Fig. 5(b), the resonance feature at 11 μm remains very similar, whereas the Wood's anomaly at the diffraction edge ($6\sqrt{2}$ μm) varies somewhat. It can be concluded that the resonance features at 11 μm in Fig. 5(b) are due to the dipole-like nature of the 5.0-μm $\times$ 0.5-μm slots [the longer slots in Fig. 5(a)].

One would expect that the shorter slots in Fig. 5(a) would also exhibit a dipole-like resonance. This second resonance is not evident in Fig. 5(b), because the expected resonant wavelength λ_r would be at a wavelength less

than the diffraction edge wavelength of $6\sqrt{2}$ μm and is masked by the spectral characteristic of the diffractive nature of the array. However, for $a_2 > 3.50$ μm, this second resonance structure is clearly visible [Fig. 5(c)].

Compton *et al.*[24] present optical transmission properties of arrays whose elements are apertures in the shape of crosses. They varied the aperture geometry, periodicity, and thickness of the mesh to determine the effects on optical performance. They found that when they increased the grid thickness for the array of crosses, the spectral width of the Wood's anomaly was broadened, effectively becoming a second passband. When combined with the inherent resonance characteristic of the crossed slots, the mesh displays a double-bandpass feature. Although the spectral characteristic shown in their paper is similar to Figs. 5(b) and 5(c) in this paper, it should be noted that the double-resonance feature shown in Fig. 5(c) is due not to a Wood's anomaly but rather to the inherent resonance properties of the two different-length apertures.

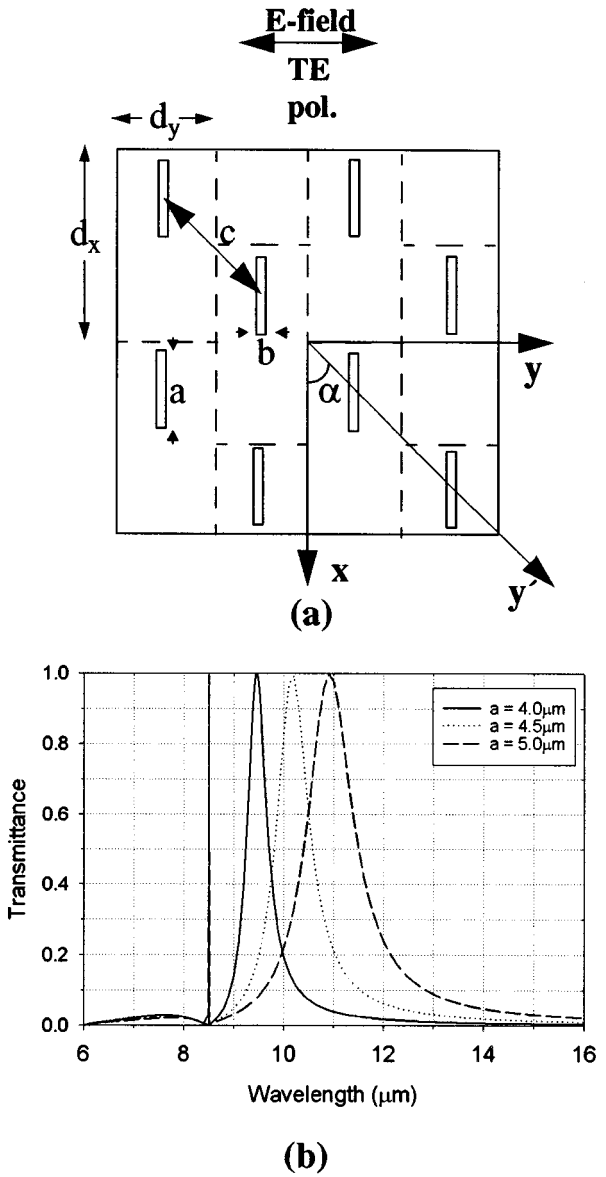

Fig. 7. (a) Typical geometry of a FSS consisting of a triangular array of a single aperture per periodic cell used for baseline comparisons. (b) Zeroth-order transmission spectral profiles for (a). In this example, $b = 0.5$ μm was held constant, and $d_x = 12.0$ μm, $d_y = 6.0$ μm, and $\alpha = 45°$ (resulting in a nearest-neighbor distance of $c = 6\sqrt{2}$ μm).

E. Effects of the Triangular Array Pattern

As a final study, we investigated the spectral profiles that result when slots are arranged in a triangular array as shown in Fig. 7(a). The resulting spectral profiles are shown in Fig. 7(b) for slot lengths of 4.0, 4.5, and 5.0 μm. The nearest-neighbor distance (periodicity) is $6\sqrt{2}$ μm, resulting in a diffraction edge at this wavelength. Examination of Fig. 7(b) clearly shows the resonant nature of the spectral profiles, with the resonant wavelength depending on slot length. One also observes that all spectral profiles are pinned at a value of zero at the diffraction edge. Since the spectral curve shifts to shorter wavelengths as the slot length shortens, the effect is a narrowing of the bandwidth with shorter slot lengths.

Comparison of the transmission spectral profiles for the triangular arrays shown in Fig. 7(b) with those in Fig. 5(c) lead to the conclusion that the dipole-like nature of the shorter slots in Fig. 5(a) causes the shorter-wavelength resonance structure in the dual-resonance transmission spectral profiles. The dual-resonance transmission spectral profiles in Fig. 5(c) are not an exact superposition of the results from the individual short-slot arrays and long-slot arrays, because of the coupling effect between the long and the short slots in Fig. 5(a). It should also be noted that although the diffraction edge is still at $6\sqrt{2}$ μm in Fig. 5(c), at least 88% of the power was in the zeroth order for all points calculated between 6.0 and $6\sqrt{2}$ μm for a_2 between 3.75 and 5.0 μm. (In fact, this jumps to 96% when $a_2 = 3.75$ μm is excluded). Even though multiple orders are propagating in this wavelength region, most of the energy resides in the zeroth order, thus reducing the possible effect of anomalies. This should be expected since the length of the shorter slots is approaching that of the longer slots. When $a_2 = 5.0$ μm, the baseline array is obtained (all slots are 5.0 μm $\times$ 0.5 μm), and the diffraction edge is then 6.0 μm.

4. CONCLUSION/EXTENSIONS

We have developed and demonstrated a method for analyzing frequency-selective surfaces with multiple apertures within a periodic cell based on an extension of the modal method developed by Chen. The technique described here can be used for any aperture shape. However, computational time in determining the coupling coefficients is significantly reduced if an analytic expression for the integral in Eq. (5) exists. In the process of investigating the viability of this numerical method, we uncovered some interesting dual-resonance transmission spectral profiles that might be useful in infrared astronomy or in target identification.

Although this paper dealt only with rectangular apertures, the program can also model circular geometries, as well as complementary structures (metallic patches instead of apertures). We plan to further investigate mix-

ing circular and rectangular apertures, as well as their complementary structures. A mixture of dipole-like structures and nonresonant elements such as circular apertures or large square apertures will permit the investigation and use of a much wider range of mesh geometries, resulting in a wider range of useful transmission spectral profiles.

ACKNOWLEDGMENT

The authors thank Robert O. Miller for many helpful discussions regarding optical properties of periodic arrays.

REFERENCES

1. R. Ulrich, "Far-infrared properties of metallic mesh and its complementary structure," Infrared Phys. **7**, 37–55 (1967).
2. C. C. Chen, "Transmission of microwave through perforated flat plates of finite thickness," IEEE Trans. Microwave Theory Tech. **MTT-21**, 1–6 (1973).
3. R. Mittra, C. H. Chan, and T. Cwik, "Techniques for analyzing frequency selective surfaces—a review," Proc. IEEE **76**, 1593–1615 (1988).
4. J. P. Montgomery and K. R. Davey, "The solution of planar periodic structures using iterative methods," Electromagnetics **5**, 209–235 (1985).
5. T. K. Wu, ed., *Frequency Selective Surface and Grid Array* (Wiley, New York, 1995).
6. R. Petit, ed., *Electromagnetic Theory of Gratings* (Springer-Verlag, Berlin, 1980).
7. B. A. Munk and R. J. Luebbers, "Reflection properties of two-layered dipole arrays," IEEE Trans. Antennas Propag. **AP-22**, 766–773 (1974).
8. C. C. Chen, "Transmission through a conducting screen perforated periodically with apertures," IEEE Trans. Microwave Theory Tech. **MTT-18**, 627–632 (1970).
9. N. Amitay, V. Galindo, and C. P. Wu, *Theory and Analysis of Phased Array Antennas* (Wiley-Interscience, New York, 1972), pp. 307–309.
10. R. Mittra, "Relative convergence of the solution of a doubly infinite set of equations," J. Res. Nat. Bur. Stand. Sect. D **67D**, 245–254 (1963).
11. C. C. Chen, "Diffraction of electromagnetic waves by a conducting screen perforated periodically with circular holes," IEEE Trans. Microwave Theory Tech. **MTT-19**, 475–481 (1971).
12. C. C. Chen, "Scattering by a two-dimensional periodic array of conducting plates," IEEE Trans. Antennas Propag. **AP-18**, 660–665 (1970).
13. J. P. Montgomery, "Scattering by an infinite periodic array of thin conductors on a dielectric sheet," IEEE Trans. Antennas Propag. **AP-23**, 70–75 (1975).
14. D. H. Dawes, R. C. McPhedran, and L. B. Whitbourn, "Thin capacitive meshes on a dielectric boundary: theory and experiment," Appl. Opt. **28**, 3498–3510 (1989).
15. S. T. Chase and R. D. Joseph, "Resonant array bandpass filters for the far infrared," Appl. Opt. **22**, 1775–1779 (1983).
16. R. W. Wood, "On a remarkable case of uneven light in a diffraction grating," Philos. Mag. **4**, 396–402 (1902).
17. Lord Rayleigh, "Note on the remarkable case of diffraction spectra described by Prof. Wood," Philos. Mag. **14**, 60–65 (1907).
18. R. W. Wood, "Diffraction gratings with controlled groove form and abnormal distribution of intensity," Philos. Mag. **23**, 310–317 (1912).
19. R. W. Wood, "Anomalous diffraction gratings," Phys. Rev. **48**, 928–936 (1935).
20. A. Hessel and A. A. Oliner, "A new theory of Wood's anomalies on optical gratings," Appl. Opt. **4**, 1275–1296 (1965).
21. R. J. Leubers and B. A. Munk, "Some effects of dielectric loading on periodic slot arrays," IEEE Trans. Antennas Propag. **AP-26**, 536–542 (1978).
22. C. H. Palmer and F. W. Phelps, Jr., "Grating anomalies as a local phenomenon," J. Opt. Soc. Am. **58**, 1184–1188 (1968).
23. C. H. Palmer, Jr., "Diffraction grating anomalies. II. Coarse gratings," J. Opt. Soc. Am. **46**, 50–53 (1956).
24. R. C. Compton, R. C. McPhedran, G. H. Derrick, and L. C. Botten, "Diffraction properties of a bandpass grid," Infrared Phys. **23**, 239–245 (1983).